ELSEVIER

Biochimica et Biophysica Acta 1371 (1998) 265–283

BIOCHIMICA ET BIOPHYSICA ACTA
BBA

Structural investigations of basic amphipathic model peptides in the presence of lipid vesicles studied by circular dichroism, fluorescence, monolayer and modeling

Cécile Mangavel [a], Régine Maget-Dana [a], Patrick Tauc [c], Jean-Claude Brochon [c], Denise Sy [a,b], Jean Antoine Reynaud [a,*]

[a] *Centre de Biophysique Moléculaire-CNRS-Rue Charles-Sadron, 45071 Orleans Cedex 2, France*
[b] *Department de Physique, Université d'Orléans, BP 6749, Orleans Cedex 2, France*
[c] *Groupe de biofluorescence, URA 1131 CNRS, Université de Paris-Sud, 91405 Orsay Cedex, France*

Received 10 February 1998; accepted 15 February 1998

Abstract

A cationic amphiphilic peptide made of 10 leucine and 10 lysine residues, and four of its fluorescent derivatives in which leucines were substituted by Trp residues at different locations on the primary sequence have been synthesized. The interactions of these five peptides with neutral anionic or cationic vesicles were investigated using circular dichroism, steady state and time-resolved fluorescence with a combination of Trp quenching by brominated lipid probes, monolayers, modeling with minimization and simulated annealing procedures. We show that all the five peptides interact with neutral and anionic DMPC, DMPG, DOPC or egg yolk PC vesicles. The binding takes place whatever the peptide conformation in solution is. In the case of DMPC bilayers the binding free energy ΔG is estimated at -8 kcal mole^{-1} and the number of phospholipid molecules involved is about 20–25 per peptide molecule. Peptides are bound as single-stranded α helices orientated parallel to the bilayer surface. In the anchoring of phospholipid head groups around the peptides, the lipid molecules are not smeared out in a plane parallel to the membrane surface but are organized around the hydrophilic face of the α helices like 'wheat grains around an ear' and protrude outside the bilayer towards the solvent. We suggest that such a lipid arrangement generates transient structural defects responsible for the membrane permeability enhancement. When an electrical potential is applied, the axis of the peptide helices remains parallel to the membrane surface and does not reorient to give rise to a bundle of helix monomers that forms transmembrane channels via a 'barrel stave' mechanism. The penetration depth of α helices in relation to the position of phosphorus atoms in the unperturbed lipid leaflet is estimated at 3.2 Å.

Keywords: Peptide; Lipid vesicle; Fluorescence; Circular dichroism; Modeling

Abbreviations: NaCl, sodium chloride; KCl, potassium chloride; Trp, tryptophan residue; Tris, tris(hydroxymethyl)amino methane; SUV, small unilamellar vesicles; LUV, large unilamellar vesicles; CD, circular dichroism; NMR, nuclear magnetic resonance; MEM, maximum entropy method; REES, red edge excitation shift; NATA, nacetyltryptophamide; DMPC, 1,2 dimyristoyl-3-phosphatidyl choline; DOPC, 1,2 dioleolyl-3-phosphatidyl choline; DMPG, 1,2 dimyristoyl-3-phosphatidyl glycerol; DMTAP, 1,2 dimyristoyl-3-trimethylammonium-propane; (6,7)BrPC, 1 palmitoyl-2-stearoyl(6-7)dibromo-3 phosphatidyl choline; (9,10)BrPC, 1 palmitoyl-2-stearoyl(9-10)dibromo-3-phosphatidyl choline; (11,12)BrPC, 1 palmitoyl-2-stearoyl(11-12)dibromo-3 phosphatidyl choline

* Corresponding author. Fax: +33-2 38 63 15 17; E-mail: jreynaud@cnrs-orleans.fr

0005-2736/98/$19.00
PII S0005-2736(98)00026-1

1. Introduction

Interactions of numerous peptides with biomembranes play a key role in many biological processes and are known to affect both peptide and membrane structural organization. A non-exhaustive list of peptides of biological significance in this context is the following: viral protein fragments, cytolytic peptides, several peptide hormones, some neuropeptides, serum protein fragments and signal peptides.

Most of these various peptides of 15- to 30-residue long stretch are amphiphilic, that is, their sequences are such that they potentially form amphiphilic α helices. The latter is a common physical feature but no homology can be detected in their primary sequence (for a review, see Ref. [1]).

In earlier studies [2,3], we investigated amphiphilic peptides such as $(LKKL)_4$, comprising solely leucine and lysine residues, which can mimic the behavior of cytolytic peptides when interacting with membranes [4–7]. The main conclusions from our investigations concerning this peptide can be summarized as follows.

(i) $(LKKL)_4$ interacts strongly with dimyristoyl phosphatidyl choline (DMPC) small vesicles (SUVs), (ii) in the presence of peptides, fusions are observed between SUVs when the molar ratio R_i is greater than 500, and a clearance effect is observed when R_i is less than 500, (iii) the efflux of carboxyfluorescein, previously encapsulated in the vesicles, in the presence of polypeptide argues strongly in favor of pore formation or transient structural defects, (iv) the num-

A

P0	L	K	K	L	L	K	K	L	L	K	L	L	K	K	L	L	K	K	L	K
PW1	W	--	--	--	--	--	--	--	--	--	--	--	--	--	--	--	--	--	--	--
PW5	--	--	--	--	W	--	--	--	--	--	--	--	--	--	--	--	--	--	--	--
PW9	--	--	--	--	--	--	--	--	W	--	--	--	--	--	--	--	--	--	--	--
PW16	--	--	--	--	--	--	--	--	--	--	--	--	--	--	--	W	--	--	--	--

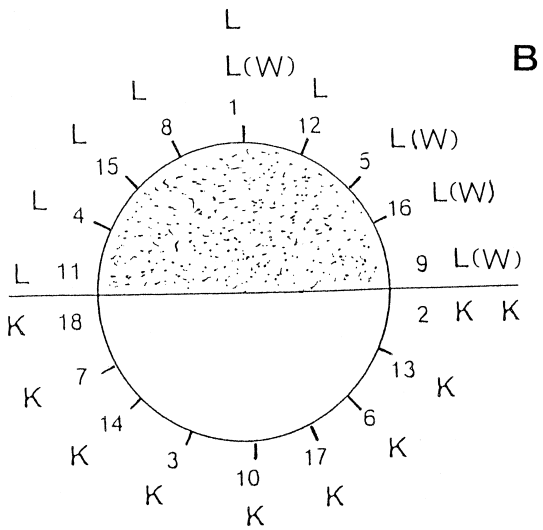

Fig. 1. (A) Amino Acid sequences of five designed amphiphilic peptides. (B) Helical wheel representation of the studied peptides and location of tryptophan residues substituted for leucines. The dotted area represents the hydrophobic part of the α helix.

ber of phospholipid molecules involved in the interaction is close to one per amino-acid residue, (v) the polypeptides adopt an α-helical conformation with their axes parallel to the membrane surface, (vi) the peptides are anchored on DMPC molecules at the negative phosphate groups through electrostatic interactions with the terminal NH_3^+ of the lysine residues, (vii) choline methyl groups are not involved in the interactions between lipid molecules and amino acid residues, (viii) phosphorus atom mobility around the *P-O*-glycerol bond is strongly reduced, whereas that of methylene groups is progressively weakened on going from C_{13} to C_1.

In this paper, we address three fundamental questions that arise concerning this kind of interaction

1. Are the peptides single-stranded or oligomeric helices when bound to a membrane and what is the orientation and the depth of penetration?
2. What is the structural perturbation brought about by membrane peptide binding on the lipid organization?
3. How sensitive are the peptide location and reorientation to a transmembrane potential?

In an attempt to answer these questions, the behavior of a 20-amino-acid long peptide P_0 made of 10 lysine and 10 leucine residues (Fig. 1) was investigated in the presence of lipid bilayers. Likewise four other peptides named PW_1, PW_5, PW_9 and PW_{16} were synthesized, in which a leucine residue was substituted by a tryptophan chromophore at different locations so that fluorescence [8] could be used in combination with circular dichroism, monolayers and modeling techniques.

2. Materials and methods

2.1. Chemicals

All reagents purchased from Merck were of analytical grade and used without further purification.

2.2. Peptide synthesis

Peptides were prepared by solid-phase synthesis using a Fmoc/Pam resin strategy in an automatic synthetisor (Applied Biosystem model 433A). The amino-acid functions of lysine and tryptophan residues were selectively protected by BOC moieties. Cleavage from the resin was achieved by treatment with TFA (95%, w/w). After deprotection of lysine and tryptophan side chains, the free peptides were purified by HPLC on a C18 lichrospher column from Vydac (USA) using an acetonitrile–water–TFA gradient system. The pure peptides were then recovered by lyophilisation. Molecular weights determined by mass spectrometry (electrospray) were 2545 D for the four tryptophan-containing peptides, a value identical to the theoretical one. The concentration of peptides with a tryptophan residue was obtained from the absorbance at 280 nm using the extinction coefficient of 5600 M^{-1} cm^{-1} or by weighing and using an extinction coefficient of 3200 at 205 nm for the peptide without tryptophan.

2.3. Lipids

All the lipids were purchased from Avanti (USA) and used without further purification.

2.4. Formation of SUVs

Vesicles were obtained by sonicating aqueous lipid suspensions (33 mg ml^{-1}) [9]. They were examined by electron microscopy (Siemens Elmiskop 102) after negative staining with 2% sodium tungstate. More than 85% of the vesicles had a diameter between 18 and 25 nm.

2.5. Formation of large unilamellar phospholipid vesicles

Large unilamellar vesicles were obtained by extrusion of multilamellar vesicles of egg yolk PC (extruder from Cipex, Vancouver, Canada) through polycarbonate filters with a pore size of 100 nm according to a protocol developed by Hope et al. [10].

2.6. Phospholipid monolayers

Penetration experiments into lipid monolayers were performed at constant area in a thermostated (20 ± 0.2°C) glass dish, as described previously [11]. Briefly, the lipids were spread out at the air/water interface from a chloroform/methanol 2:1 mixture to give the desired initial pressure Π_i. An amount of the peptide stock solution was injected underneath the

lipid film. The change in surface tension was recorded by the Wilhelmy platinum plate method with an accuracy of ± 0.5 mN m^{-1}.

2.7. Membrane potential

In order to produce the Na^+/K^+ chemical gradient required to establish a membrane potential, LUVs were made in a buffered medium (149 mM KCl, 1 mM NaCl, 10 mM Tris, pH 7.1). Subsequently, the untrapped buffered medium was exchanged for a buffered solution (149 mM NaCl, 1 mM KCl, 10 mM Tris, pH 7.1) by passage through a Sephadex G-50 column which was pre-equilibrated with the latter solution. Transmembrane potential was generated by adding a minute amount of valinomycin in DMSO (1 $\mu g \cdot PC\,\mu mol^{-1}$) and the potential time course was routinely monitored by following the maximum fluorescence intensity of 3,3′-dipropylthiocarbo-cyanine ($\lambda_{em} = 680$ nm, $\lambda_{ex} = 620$ nm), a potential sensitive probe [12]. This method enabled a qualitative assessment of the establishment and of the dissipation extent of the membrane potential. Transmembrane potential $\Delta\psi$ was calculated employing the Nernst equation:

$$\Delta\psi = -0.059 \log[K_i^+]/[K_0^+],$$

$[K_i^+]$ and $[K_0^+]$ being the K^+ concentration inside and outside the vesicles, respectively.

2.8. Optical spectroscopy

Circular dichroism (CD) spectroscopy was performed on Jobin Yvon Autodichrograph Mark V. Ellipticity was expressed as a mean residue ellipticity $[\theta]$ with the units $deg \cdot cm^2 \cdot dmol^{-1}$, the sample concentration was maintained between 11 and 13 μM. Baseline spectra for each solvent were obtained prior to the peptide spectra and mean ellipticity values per residue were calculated after subtracting the corresponding base line. The peptide α helicity percentage was estimated as:

$$\frac{[\theta]_{222}}{[\theta]_{222}^{max}} \times 100$$

where $[\theta]_{222}$ was the observed mean ellipticity per residue at 222 nm and $[\theta]_{222}^{max}$ was the maximal theoretical ellipticity at 222 nm which was calculated from the relationship: $-39{,}600\ [1 - 2.6/20] = -34{,}400$ deg cm^2 $dmol^{-1}$, 20 being the number of residues per peptide molecule [13].

Steady state fluorescence spectra were recorded on a 3C Jobin–Yvon spectrofluorimeter. All fluorescence measurements were made with an excitation wavelength of 280 nm on solutions of optical density < 0.1 with a slit width of 2 nm or 4 nm in the case of LUVs and the path length of the cell was 1 cm. Fluorescence was expressed in arbitrary units after subtracting the corresponding base line of the solvent spectra.

Fluorescence decays were measured by the time-correlated single photo-electron counting technique [14,15]. The optical and electronic set-up have been previously described [16]. The excitation light pulse at 290 nm was generated by the third harmonic generation of a Ti sapphire subpicosecond laser (Tsunami, Spectra Physics) The repetition of the laser was set down to 4 MHz. The fluorescence emission was detected through a monochromator Jobin–Yvon H 10 (Dl = 8 nm) by a microchannel plate photomultiplier (Hamamatsu R1564U-06). The instrumental response function was recorded by detecting the light scattered by a water solution. The time scaling was 29 ps per channel and 1200 channels were used. The fluorescence decay and the instrumental response profile were collected and stored every 240 s and 30 s alternatively until the total counts or the fluorescence decay reached 7–8 million. The samples were thermostated at 30°C. Analysis of the fluorescence decays was performed by the Quantified Maximum Entropy Method (MEM) [17,18].

All CD or fluorescence spectra were the average of three scans. A HAAKE thermostat (type 4391) was routinely used to control the temperature of the cell. Moreover all measurements were performed in degassed media by nitrogen bubbling.

2.9. Modeling

The modeling study was carried out with SYBYL software (Tripos, St Louis, MO, USA). For calculations the Tripos force field was used with the following specifications, i.e., Pullman charges and distance dependent dielectric constant in order to mimic the solvent. The following procedure was applied to the study of the peptide P_0 in a lipid environment.

First, an assembly of 24 DMPC lipids was built and energy minimized. The peptide in an α-helical conformation was then merged in the middle of the polar head region of the lipid assembly. The resulting structure was submitted to a new energy minimization with initial distance constraints between the lipid phosphate groups and the lysine amino groups in order to favor electrostatic interactions. Due to these minimization steps, the lipids were in a gel-like phase and a void was present in the region neighboring the hydrophobic area of the peptide. In order to explore a larger conformational domain [19] and thus to correct this unrealistic situation, a simulated annealing procedure was carried out on the whole structure, that is the system is 'heated' to a high temperature where torsional energy barriers can be overcome then slowly 'cooled' to a low temperature where the system is trapped in a potential well. During this procedure, the 10 outermost lipids were maintained fixed and the following conditions were used: equivalent upper temperature 700 K during 1000 fs followed by an exponential decrease to 200 K for 1000 fs and further minimization; only assemblies where the peptide kept a helical structure were retained.

For various initial locations of the peptide embedded inside the lipid assembly, the whole system was then submitted to energy minimization in order to obtain the final structures. For the depth penetration analysis, a reference plane was defined from the average position of the phosphorus atoms belonging to the outermost lipids, whereas the peptide position was defined by the centroid of the backbone atoms (middle of the helix axis). The initial and final distances of the peptide centroid to the reference plane were named d_i and d_f, respectively.

3. Results

3.1. Circular dichroism

In pure water the peptides are mainly in random coil conformation [20] (Table 1). In various mixtures containing suspensions of DMPC vesicles (SUV) at 30°C, 1 mM Tris, pH 7.1, all the CD spectra obtained for the different peptides are very similar. In Fig. 2, several spectra of PW_1 corresponding to different ratios R_i ([lipid concentration]/[peptide concentration]) are shown. When R_i is large, CD spectra display two minima at 208 and 222 nm characteristic of a right-handed α helical conformation due to the peptide binding to the vesicle bilayers. The presence of an isodichroic point at 204 nm and the value of the ratio $[\theta]_{222}/[\theta]_{208}$ close to 0.8 argue strongly in favor of the peptide monomer insertion as single stranded helices [21,22]. Mean residue ellipticity limits at 222 nm, obtained when R_i tends to the infinite (Fig. 3), and the associated helical percentages for P_0, PW_1, PW_5, PW_9 and PW_{16} are presented in Table 1. For peptides P_0, PW_1, PW_5 and PW_{16} the helical content is higher than 90%, but that of PW_9 does not exceed 73%. Such behavior is strongly reminiscent of that exhibited in TFE medium (Mangavel et al. [20]) and confirms the tryptophan helix destabilizing effect when this residue is located in the middle of the hydrophobic faces of an amphiphilic peptide.

3.2. Estimation of the binding free energy from the binding constant

To determine an apparent binding constant K of P_0, PW_1, PW_5, PW_9 and PW_{16} to DMPC vesicles, the

Table 1
The mean residue ellipticity limits of peptides at 222 nm and fluorescence emission maxima of PW_0, PW_1, PW_5, PW_9 and PW_{16}, in pure water, in salted solutions (0.1 M $NaClO_4$) and in suspensions of DMPC vesicles (SUV) in 1 mM Tris, pH 7.1 at 30°C

Peptide	Pure water		Salted solution		SUV (DMPC)	
	$[\theta]_{222}$ (deg cm^2 dmol^{-1})	λ_{max} (nm)	$[\theta]_{222}$ (deg cm^2 dmol^{-1})	λ_{max} (nm)	$[\theta]_{222}$ (deg cm^2 dmol^{-1})	λ_{max} (nm)
PW_1	−4100	356	−29,000	347	−31,000	328
PW_5	−3700	356	−31,000	344	−31,000	327
PW_9	−3000	356	−29,000	346	−25,000	330
PW_{16}	−3500	356	−30,000	346	−33,000	331

All values were the limits obtained by extrapolation of R_i tending to the infinite for peptides in vesicle suspensions.

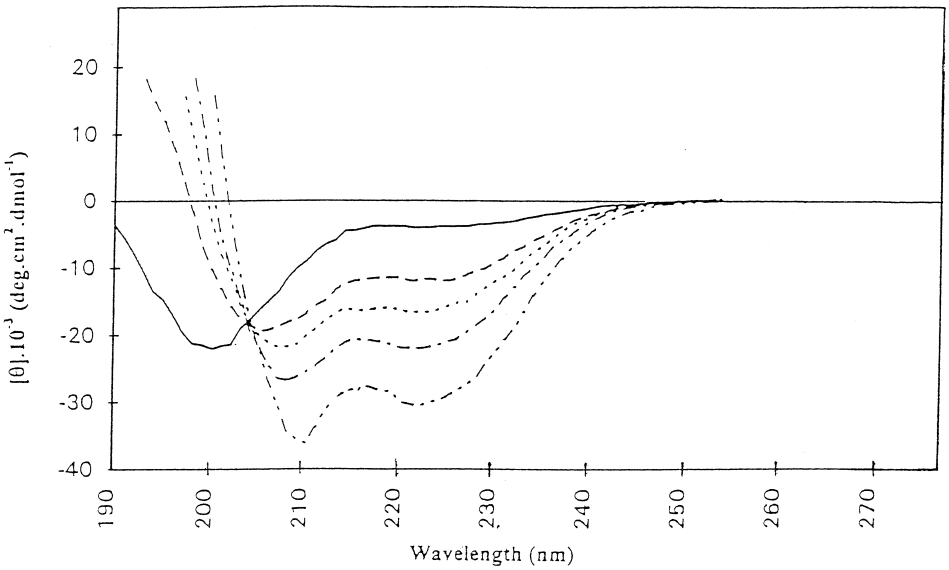

Fig. 2. The CD spectra of PW_1 in aqueous solution (————) and in vesicle suspensions of DMPC for various values of the concentration ratio R_i(= [lipid]/[peptide]). From top to bottom at 222 nm R_i is successively equal to 0, 120, 180, 250 and 980. Peptide concentration was kept constant 12 μM. All the spectra were recorded at 30°C, in 1 mM Tris, pH 7.1, using 0.5-cm cell.

binding data were analyzed according to the Langmuir adsorption isotherm [23]:

$$r/C_f = K(1/N - r) \quad (1)$$

where C_f is the free peptide concentration; N is the number of lipid molecules interacting with one peptide molecule, $r = C_b/0.6\ C_L$ is the number of peptide molecules adsorbed per lipid molecule (the factor 0.6 accounts for the asymmetry in the lipid concentration in the outer and in the inner layers of vesicles as suggested by Beschiasvili and Seelig [24]); C_b is the concentration of bound peptides and C_L is the analytical concentration of lipid molecules.

It should be noted that such an isotherm described by Eq. (1) is strictly valid for the binding of ligands covering independent sites with no overlapping onto the lipid bilayers [25]. Although in our case these experimental conditions are not completely fulfilled, if R_i is large we can make the assumption that the total number of binding sites greatly exceeds the peptide concentration, then, in rough approximation, Eq. (1) remains valid.

Lipid titrations were carried out by adding small amounts of concentrated lipid vesicle suspension to the peptide solutions, the concentrations of which were maintained constant (12 μM). The bound peptide concentrations for different R_i values were determined from CD spectra at 222 nm using the formula:

$$C_b = 12.10^{-6}\frac{[\theta] - [\theta_0]}{[\theta]_{lim} - [\theta_0]}$$

where $[\theta]$ was the measured mean residue ellipticity of the peptides in the presence of lipid vesicles, $[\theta_0]$ and $[\theta]_{lim}$, respectively the mean residue ellipticity in the absence and in the presence of lipid when all the peptide was bound onto the lipid bilayer (Fig. 3 and Table 1). The different values of the association constant K and of the number N of lipid molecules interacting with a single peptide molecule were determined by the Scatchard's plot r/C_f vs. r. A typical plot for PW_1 is shown in the insert of Fig. 3. In view of the broad margin of error due to the use of Langmuir's isotherm, no significant difference can be detected for either K or N. The values of K ranged from 10^5 to 10^6 M^{-1} and N from 10 to 20 phospholipid molecules. The K estimation is in good agreement with those obtained from monolayer experiments on $(Leu\text{-}Lys\text{-}Lys\text{-}Leu)_4$ peptides (Maget-Dana, unpublished results) or other results on amphipathic peptides from the literature [26]. Calculated from K, the free energy value ΔG, was close to -8 kcal M^{-1}. This high value can be explained as follows: amphipathic peptide binding onto lipid vesicles is

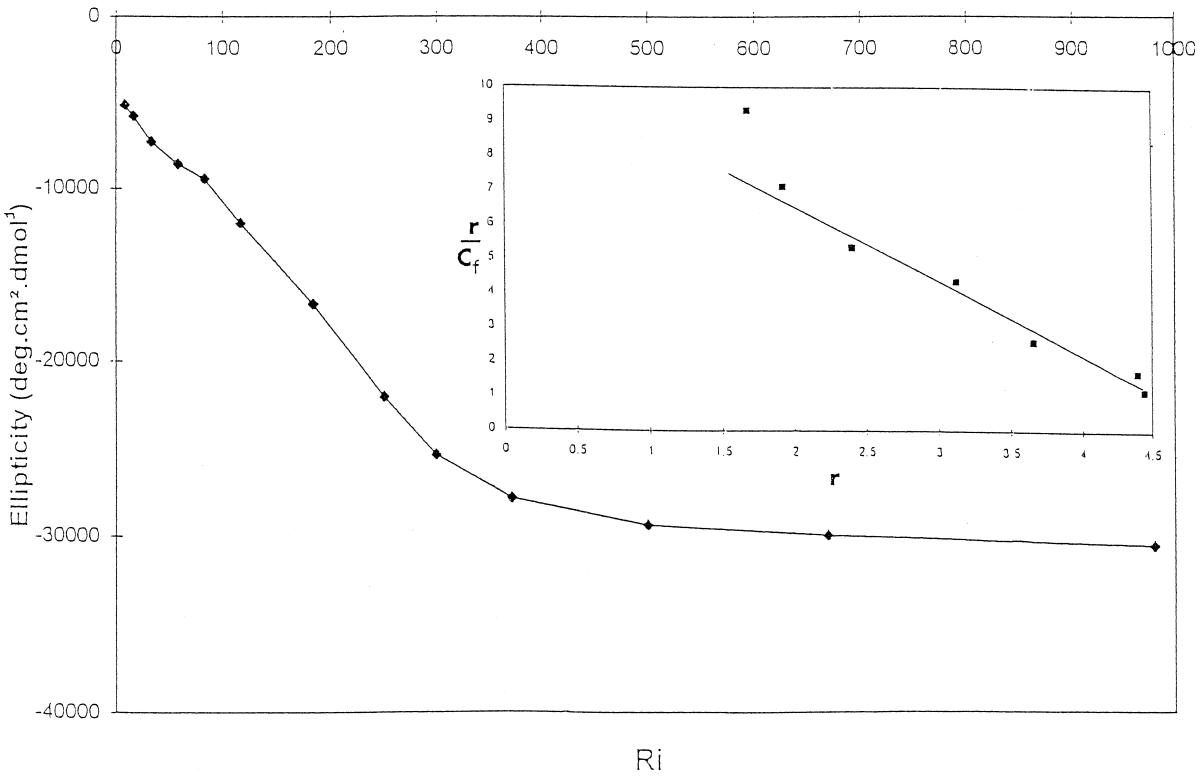

Fig. 3. The mean residue ellipticity of PW_1 at 222 nm in vesicle suspensions of DMPC for various ratios R_i = [lipid]/[peptide], in 1 mM Tris, pH 7.1 at 30°C. Peptide concentration 12 μM, 0.5 cm cell. Insert: corresponding Scatchard plot of PW_1. The solid line represents the best linear regression fit to the data. The ratio r/C_f is expressed in mM^{-1}, where $r = C_b/0.6\ C_L$ is the number of peptide molecules adsorbed per lipid molecule with C_b the bound peptide concentration, C_L the analytical concentration of lipid molecules, and C_f the free peptide concentration.

driven by two kinds of forces called hydrophobic (or entropic forces) and electrostatic forces due to the strong interaction between positive lysine residues and negative lipid phosphates. In our case, the latter phenomenon which depends on the number of lysine residues, should give rise to a high binding energy.

3.3. Peptide binding on anionic or cationic lipids

Interactions of the five peptides with negatively charged vesicles, DMPC:80, DMPG:20 (m/m), resulted in a very strong increase of turbidity even for R_i values higher than 2000. Nevertheless, CD spectra retained a typical behavior of α helix conformation but the large light scattering, resulting from vesicle aggregation and/or fusion, prevented any other spectroscopic measurements from being further processed.

Electron microscopy photographs (not shown) clearly evidenced the occurrence of large multilayered vesicles resulting from the peptide-induced fusion of small unilamellar vesicles. This phenomenon, already encountered with small unilamellar DMPC vesicles, was enhanced in the presence of anionic vesicles due to the negative charges borne by the vesicles that increased the peptide accumulation at the bilayer surface.

In contrast with the previous experiments, in suspensions of cationic vesicles of DMTAP, no peptide binding was observed. In Fig. 4 the CD spectra of PW_9 are typical of random coil conformation, whatever the R_i values be.

These data emphasize the conspicuous role of the electrostatic interactions in the peptide binding to lipid bilayers since when the electrostatic interaction between positively charged lysine residues and negatively charged phosphate groups does not exist

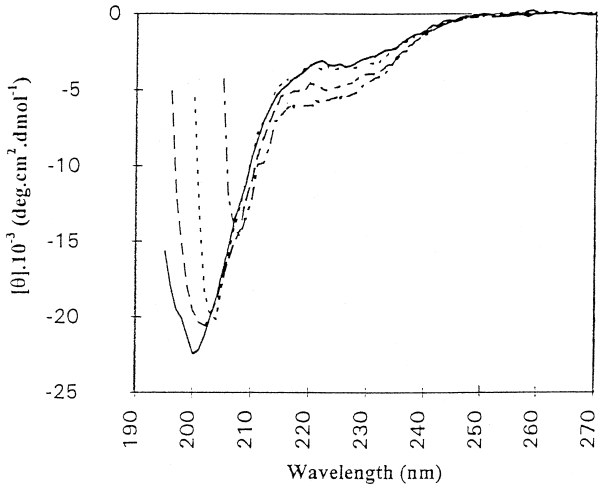

Fig. 4. The CD spectra of PW_9 in aqueous solution (————) and in suspensions of cationic vesicles of DMTAP for various values of the concentration ratio R_i = [lipid]/[peptide]. From top to bottom, R_i is successively equal to 47, 173 and 364. Peptide concentration was kept constant 12 μM, 1 mM Tris, pH 7.1, 0.5 cm cell at 30°C.

(DMTAP) the peptide binding cannot occur. This strongly suggests a two-step mechanism involving first, electrostatic interactions between phosphate moieties and lysine residues and second, clustering of leucine residues driven by hydrophobic forces into a less polar region of the bilayer.

3.4. Steady state fluorescence measurements

Interactions of PW_1, PW_5, PW_9 and PW_{16} with vesicles of DMPC resulted in an enhancement of Trp fluorescence intensity and a blue shift of the emission maximum (Fig. 5A and B) as expected when the tryptophan residue moves from an aqueous phase to a less polar environment [27].

In Fig. 6A, the emission maximum wavelength dependence with the Trp residue distance to the median plane separating the hydrophobic face from the hydrophilic face of the α helix (Fig. 6B) indicates that the peptides are bound with their helical axis parallel to the plane of the bilayer, as suggested by the rank order $\lambda(PW_9) > \lambda(PW_{16}) > \lambda(PW_5) > \lambda(PW_1)$. As a matter of fact, if the helical axis were perpendicular to the bilayer, the rank order of the emission maxima would be $\lambda(PW_1) > \lambda(PW_5) = \lambda(PW_{16}) > \lambda(PW_9)$. Besides, we can notice that such a location is unlikely to occur since 10 hydrophilic lysines bearing one positive electrical charge would be in tight contact with the hydrophobic lipid phase. This is thermodynamically impossible. The only possibility for an amphipathic α helix to settle in perpendicular orientation is to associate with other α helices and to form a transbilayer bundle. In this structure, the hydrophobic leucine residues are surrounded by hydrophobic acyl chains and hydrophilic lysine residues by the solvent. In this case the distance from W_5 and W_{16} to N- and C-termini remains identical but W_5 is nearer to the solvent than W_9 which is totally buried in the hydrophobic phase. Therefore the order of maximum emission wavelengths would be $\lambda(PW_1) > \lambda(PW_5) > \lambda(PW_{16}) > \lambda(PW_9)$, which is different from the one experimentally observed.

3.5. Time-resolved fluorescence measurements

The fluorescence decay parameters of the four Trp containing peptides were measured at several wavelengths between 320 and 375 nm (excitation at 280 nm). In all degassed samples the tryptophan fluorescence could be resolved into three or four exponential components. The results obtained are summarized in Table 2. It is noteworthy that, in the case of free Trp, only two exponential decay times are observed [27].

The general features shared in common between the four peptides are as follows. (1) Decay times are very sensitive to the presence of oxygen acting as a Trp quencher and leading to the decrease of each decay time. This result is consistent with the observation that O_2 is much more soluble in organic solvent or membranes than it is in pure water [28]. (2) The distribution curves for each decay time (preexponential factors) consist of sharp peaks suggesting a very weak polydispersity of respective populations; such an example is shown in Fig. 7. (3) The analysis of individual decay curves indicated that the decay times could depend on the emission wavelength.

For the peptides PW_5, PW_9 and PW_{16} the three decay times ranged from 0.13 to 0.67 ns for τ_1, 1.10 to 1.57 ns for τ_2 and 3.44 to 4.21 ns for τ_3. The origin of such decays has been the subject of intensive study [29] and there is currently wide agreement that such behavior originates from the fluorescence of different rotational conformers (rotamers) of the in-

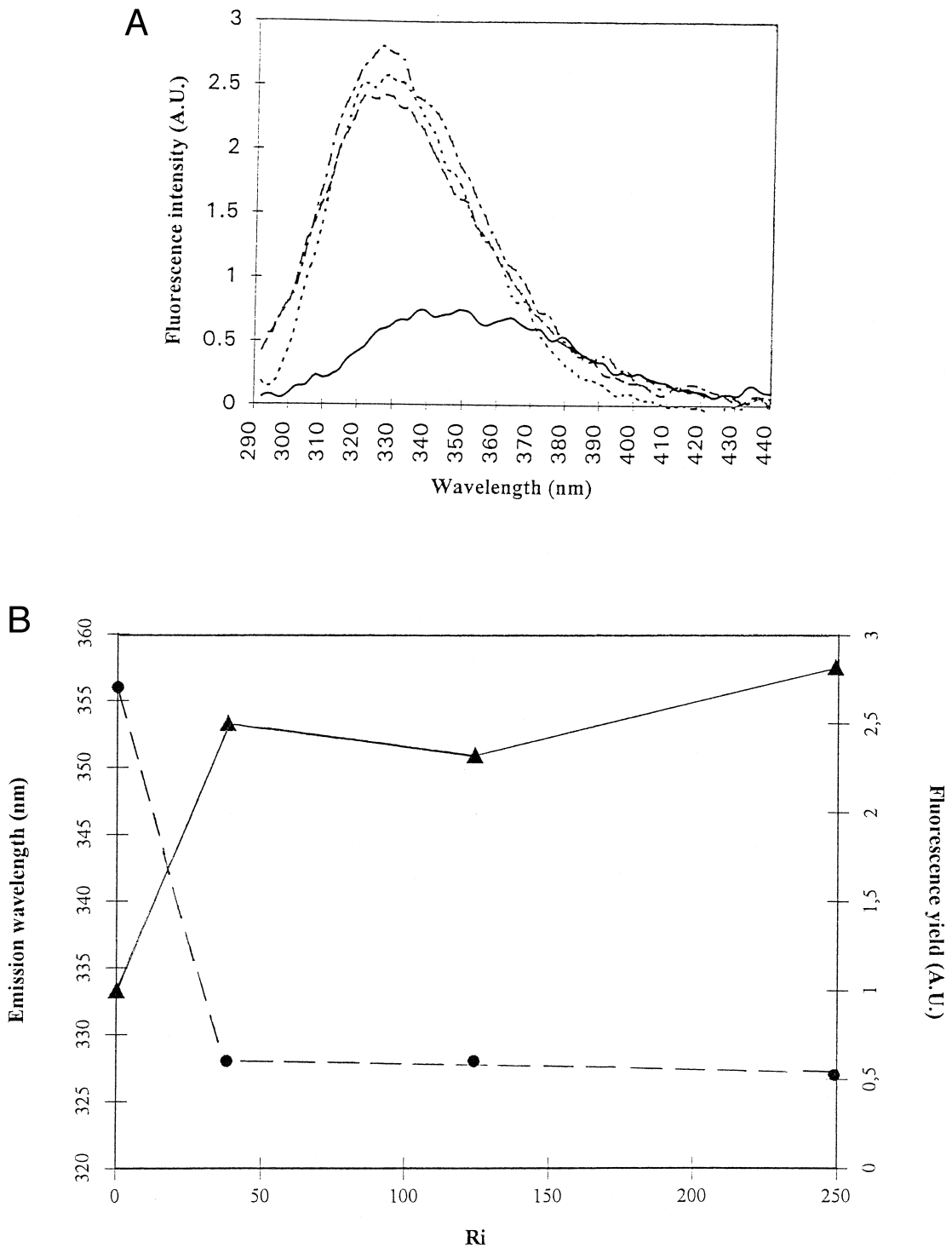

Fig. 5. (A) The fluorescence emission spectra of PW_5 ($c = 0.45$ μM) in aqueous media (————) and in the presence of DMPC SUV at 30°C, 1 mM Tris, pH 7.1, cell length 1 cm. From top to bottom R_i is 250, 124, 38 and 0. (B) Emission wavelength maximum (- - -) and fluorescence yield (————) of PW_5 variation with R_i([lipid]/[peptide]).

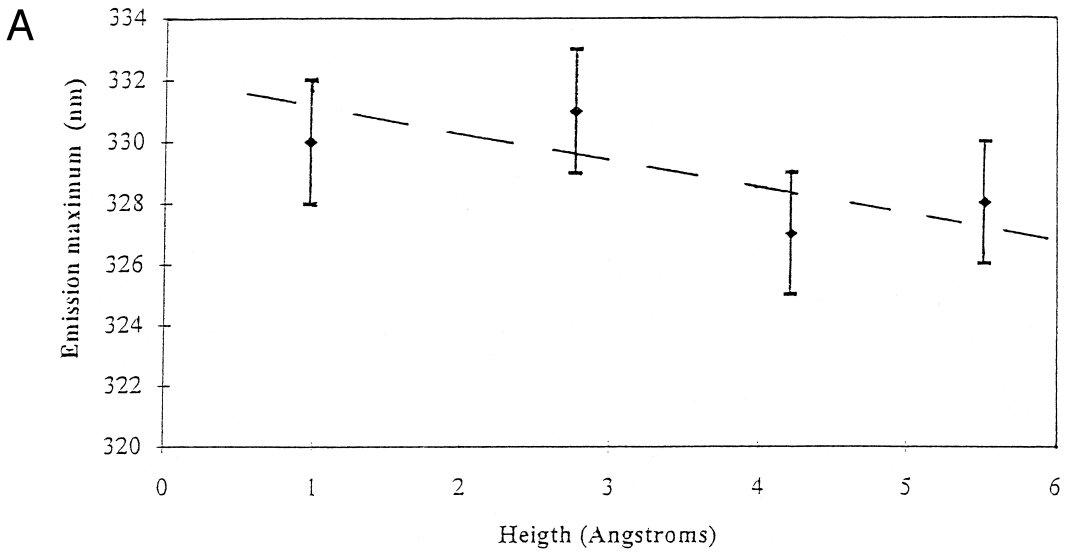

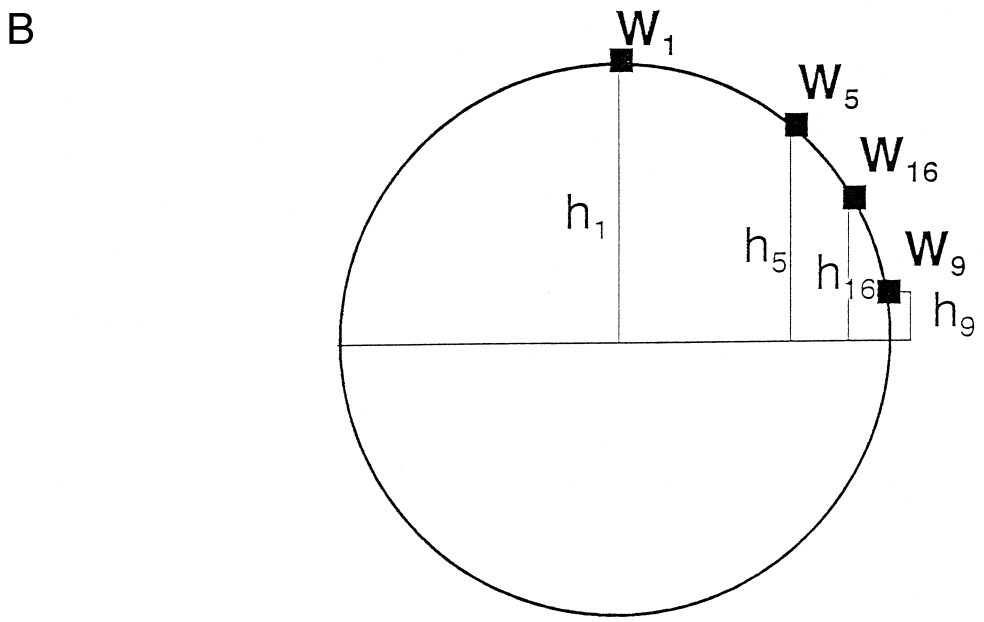

Fig. 6. (A) The emission wavelength maxima vs. location of tryptophan residue in the α helix represented by the distance of the residue to the plane separating the hydrophobic face from the hydrophilic one. (B) Tryptophan distances to the plane separating the hydrophobic face from the hydrophilic one: $h_1 = 5.5$ Å, $h_5 = 4.2$ Å, $h_{16} = 2.75$ Å, $h_9 = 0.96$ Å.

dole ring around the Cα–Cβ bond of the alanyl side chains [30–33]. For PW_1 peptide, the fluorescence decay is best described by four decay times $\tau_1 = 0.56$ ns, $\tau_2 = 1.90$ ns, $\tau_3 = 3.33$ ns and $\tau_4 = 6.10$ ns. This behavior should be connected with the location of the Trp residue at one end of the α-helix where its environment is different from that in the peptides, where Trp is located in the core of the helix.

Table 2
The lifetimes, preexponential factors and relative quantum yield ratios

PW/SUV	λ_{em} (nm)	τ_1 (ns)	τ_2 (ns)	τ_3 (ns)	τ_4 (ns)	α_1	α_2	α_3	α_4	$\langle\tau\rangle$	Q_{rel}	$\langle\tau\rangle/Q_{rel}$
PW1	330	0.56	1.90	3.33	6.10	0.12	0.38	0.33	0.17	2.90	1.8	1.60
PW5	320	0.13	1.29	4.12		0.09	0.21	0.70		3.20		
	330	0.19	1.22	4.15		0.04	0.21	0.75		3.35		
	340		1.10	4.12			0.20	0.78		3.40		
	350	0.13	1.29	4.21		0.07	0.18	0.75		3.40		
	375	0.15	1.29	4.14		0.14	0.20	0.66		3.00		
										3.30	2.9	1.14
PW5(∗)	330	0.10	0.91	1.83		0.09	0.20	0.71				
	340	0.10	0.98	1.81		0.03	0.15	0.82				
PW9	330	0.25	1.57	3.92		0.10	0.21	0.69		3.10	2.9	1.07
PW16	330	0.67	1.41	3.44		0.05	0.30	0.65		2.70	2.0	1.35
NATA	353	2.80				1.00				2.80	1.00	2.80

All peptides were in DMPC SUVs in 1 mM Tris, pH 7.1 at 30°C.
(∗) Non-degassed suspensions.

Relative fluorescence quantum yields Q_{rel} were determined using peptide/SUV suspensions with absorbance < 0.1 ($C_{PWi} = 0.45\ \mu M$) at the excitation wavelength of 280 nm. NATA in pH 7.1 Tris buffer at 30°C was used as a fluorescence quantum yield standard and exhibited single exponential decay kinetics with a life time of 2.8 ns at 30°C [27]. For the three peptides PW_5, PW_9 and PW_{16}, the Q_{rel} values are not very different from each other: 2.9, 2.9 and 2.0, respectively. These observations suggest a similar environment for the tryptophan residue in these peptides. For peptide PW_1, both decay time and relative quantum yield are different suggesting some difference in the environment and thereby in the quenching process.

In order to gain insight into the quenching mechanisms of the Trp containing peptides, the relative quantum yields were compared with the species concentration weighted lifetime $\langle\tau\rangle$ [27] where $\langle\tau\rangle = \Sigma\alpha_i\tau_i$. In dynamic quenching, where deactivation of the excited fluorophores is competitive with fluorescence, Q_{rel} is equal to $\langle\tau\rangle/\tau_{ref}$, where τ_{ref} is the lifetime of the standard. Deviations from the above equation such that $\langle\tau\rangle/Q_{rel} > \tau_{ref}$ signify static quenching which is usually due to the ground state formation of non-fluorophore complexes or the presence of self-quenched conformer, the interconversion of which is slow on the fluorescence time scale (quasi-static self quenching [30]). Table 2 shows the life time/quantum yield ratios $\langle\tau\rangle/Q_{rel}$ for Trp peptides and NATA; these ratios are smaller or equal to that of NATA, indicating the essentially dynamic nature of the quenching. At first sight, such a conclusion seems surprising because the reduced mobility of the different rotamers should lead to a static quenching of Trp fluorescence by peptidic bond [30,34,35]. In fact, due to the insertion of lipid acyl chains between the peptidic bond and the Trp sidechain [2], the electron exchange between the electron acceptor (–CO–NH) and the donor (Trp indole) is switched off. In this event, it can be thought that there is no trace of static quenching in the fluorescence of PW_1, PW_5, PW_9 and PW_{16} embedded in the outer leaflet of DMPC vesicles.

3.6. Red edge excitation shift

A shift in the wavelength of maximum emission toward higher wavelengths, caused by a shift in the excitation toward the red edge of the absorption band is termed the red edge excitation shift (REES). This effect is mostly observed with polar fluorophores in motionally restricted media such as very viscous solutions or condensed phase like membranes, that is when the fluorophore mobility relative to the surrounding matrix is considerably reduced [36,37]. Such an effect is observed with our Trp containing peptides bound to DMPC vesicles as shown in Fig. 8 and thus supports the hypothesis of strongly reduced mobility of tryptophan side chains.

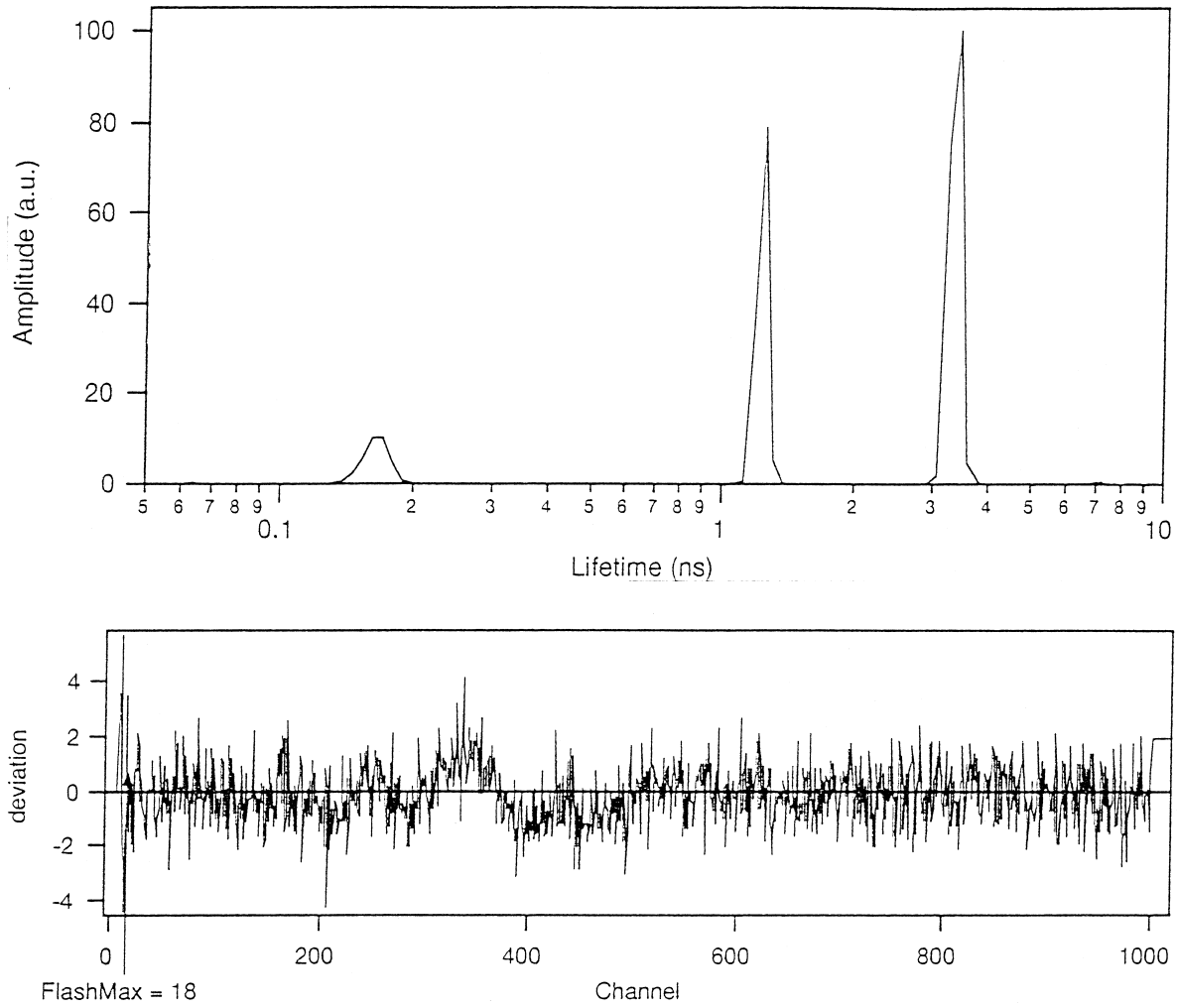

Fig. 7. The MEM reconstituted excited-state lifetime distribution of PW_5 peptide in DMPC SUVs; $\lambda_{exc} = 380$ nm and $\lambda_{em} = 330$ nm, degassed sample, R_i = [lipid]/[peptide] = 100, 1 mM Tris, pH 7.1 at 30°C.

3.7. Peptide aggregate binding to DMPC SUVs

The four peptides studied in a salted $NaClO_4$ medium generating some ionic strength gave rise to the formation of interacting structures where α helices are joined together side by side. These results displayed in Table 1 show that the red shifted emission maximum wavelengths are different from those in water and give evidence for the formation of aggregates through the intermediary of hydrophobic forces [20].

Stepwise addition of vesicle suspensions to a solution of any peptide aggregates at 30°C, pH 7.1 in 0.1 M perchlorate led to marked changes in the fluorescence spectra, characterized by an increase in fluorescence yield and blue shift of the emission maximum wavelength from 346 ± 2 nm to 329 ± 2 nm. The latter corresponds exactly to the mean emission maximum wavelength observed when peptides previously in random-coil conformation (aqueous medium) are bound as simple α-helices to vesicles. These results provide evidence for the peptide binding to vesicles through the intermediary of peptide-aggregate dissociation at the bilayer surface.

3.8. Penetration into phospholipid monolayers

To confirm the validity of this finding, measurements with DMPC monolayers were undertaken. A

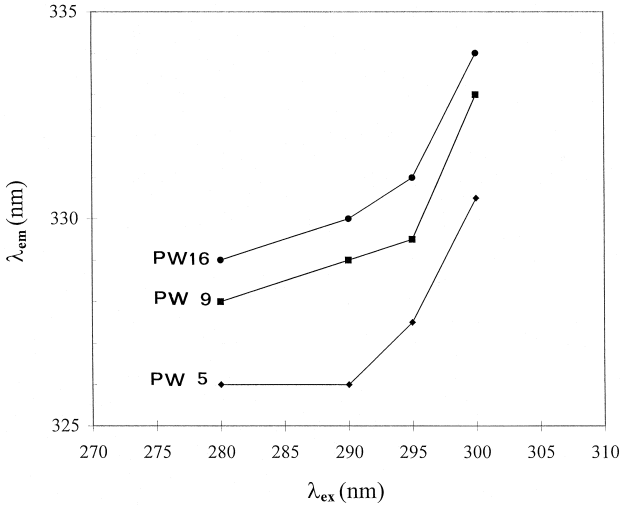

Fig. 8. The effect of changing excitation wavelength on maximum emission wavelength for peptides PW_5, PW_9 and PW_{16} in DMPC vesicles, $R_i = [\text{lipid}]/[\text{peptide}] = 100$. 1 mM Tris, pH 7.1 at 30°C.

monolayer of DMPC was spread over an aqueous subphase at an initial pressure $\Pi_i = 16 \pm 1$ mN m^{-1} and the peptide PW_5 was injected underneath, resulting in a surface pressure increase ($\Delta\Pi$) which indicated the insertion of the peptide into the phospholipid monolayer.

In Fig. 9, $\Delta\Pi$ was plotted against the PW_5 concentration, for a subphase containing salt (149 mM sodium chloride, 1 mM potassium chloride, 1 mM Tris, pH 7.1): the increase in surface pressure reached 30 mN m^{-1} at 10^{-5} M peptide concentration whereas it was only 10 mN m^{-1} in a pure water subphase.

On the other hand, the kinetics for each equilibrium to be established was fast (a few minutes) in the case of salted subphase in which the peptide formed helix aggregates, whereas it was very slow (several hours) in the case of aqueous subphases where peptides were in random coiled conformation. Such behavior needs to be explained. In this respect, it should be recalled that SUVs contain many structural defects [38,39], whereas monolayer surfaces are known to be rather smooth. Before any possible peptide anchorage to the monolayer, the repulsive barrier exerted by the positive charges of cholines against lysine residues has to be overcome; when this is the case, the phosphate groups become accessible to the lysine residues, attraction can occur and the leucine residues can move to the more hydrophobic region of the layer, leading to a further clustering of leucine residues driven by hydrophobic forces into the neighborhood of lipid alkyl chains. This requirement is met both with SUVs due to the presence of structural defects which can bring the negative phosphate groups and the positive lysine residues directly into contact, and with a monolayer where the ionic strength in the subphase can exert a screening effect against the repulsive choline barrier.

In aqueous subphases where no screening effect can arise, it can be thought that the peptide binding is made very difficult, resulting in the weakening of the binding rate and in the decrease of the amount of peptide bound. This is exactly what was experimentally evidenced.

In order to support the suggested mechanism which needs the presence of structural defects for the cationic peptide binding on a lipid layer where the repulsive choline barrier is not screened, some structural defects were artificially created in the DMPC monolayer by the injection of small amounts of pure water into the subphase. As expected (results not shown) the water injection was immediately followed by a rapid enhancement of the amount of bound peptide.

The maximum of the surface pressure at 10^{-5} M peptide concentration corresponding to the monolayer saturation was estimated at 46 mN m^{-1} from the increment pressure dependence with the PW_5 concentration (Fig. 9). In order to determine the number of lipid molecules per peptide molecule bound we made the following estimation. The number N of lipid

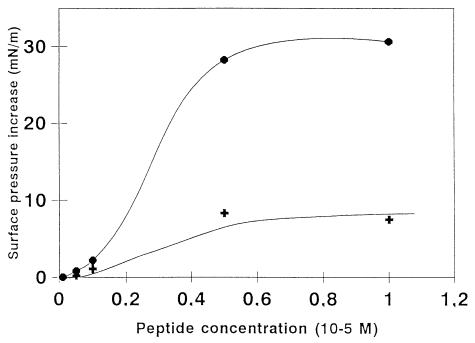

Fig. 9. Surface pressure increase of a DMPC monolayer as a function of PW_5 peptide concentration in the subphase. The initial pressure of the DMPC monolayer is 16 ± 0.5 mN m^{-1}. (+) peptide in aqueous medium and (●) in 0.1 ionic strength (149 mM NaCl, 1 mM KCl, 1 mM Tris, pH 7.1).

molecules spread as a monolayer is: N = trough area/molecular area of DMPC phospholipid head at 16 mN m^{-1} (data from the compression isotherm, not shown), i.e., $N = 1.96\ 10^{17}/72 = 2.72 \times 10^{15}$. At 46 mN m^{-1} the molecular area of DMPC phospholipid head was estimated at 42 Å^2 from the compression isotherm, thus the total area occupied by the lipids was $2.72 \times 10^{15} \times 42 = 1.14 \times 10^{17}$ Å^2. Hence the area occupied by the peptide molecules is $(1.96–1.14)10^{17} = 8.2 \times 10^{16}$ Å^2. If the area occupied by a peptide molecule bound on the monolayer can be assumed to be that of an α helix of length 30 Å and radius 6 Å, the maximum number of peptide molecules bound was $8.2 \times 10^{16}/(30 \times 12) = 2.27 \times 10^{14}$ and the number of lipid molecules per peptide molecule was estimated at $2.8\ 10^{15}/2.27 \times 10^{14} = 12$. Such a value is close to those determined by isotherm adsorption and fluorescence quenching measurements (see below).

3.9. Penetration depth of tryptophan containing peptides in DOPC SUVs

We attempted to estimate the penetration depth of the Trp containing peptides in lipid bilayers by comparing the quenching efficiency F_0/F (F_0, fluorescence intensity in absence of quencher; F in presence of quencher) by three brominated phospholipid probes noted (6,7)BrPC, (9,10)BrPC, (11,12)BrPC incorporated at different mole fractions into the bilayer of DOPC small unilamellar vesicles [40].

Data obtained for the four peptides are displayed in Table 3. (6,7)BrPC and (9,10)BrPC were the most efficient quenchers of the fluorescence intensity, and for a given probe the intrinsic fluorescence for each peptide was equally quenched whatever the Trp position in the primary sequence. At first sight such behavior could appear surprising: as a matter of fact, due to their different locations in the α helix (Fig. 6B), each Trp residue is characterized by a specific penetration depth inside the lipid leaflet and therefore the respective quenching efficiency should be modified with the Trp residue position. This is not the case since the quenching efficiency is similar whatever the Trp distance to the center of the bilayer be. What do these results mean? The fluorescence quenching bromine atoms are borne by phospholipid molecules which are anchored to the α helix by electrostatic interactions between negatively charged phosphate groups and positively charged protonated lysine residues. This results in the phosphate groups not being smeared out in a plane parallel to the membrane surface but in their becoming organized around the hydrophilic face of the α helices like ‘wheat grains around an ear’. In static quenching as is the case in the experiments (see further), tight contact is required between chromophores and quenchers. Consequently an ith Trp residue fluorescence can be quenched only by the bromine atoms borne by phospholipid molecules anchored to $i-1$ or i + 1 lysine residues and possibly by those anchored to the lysine residues located in the two adjacent α helix spirals.

Table 3
The quenching efficiency (F_0/F) of (6,7)BrPC, (9,10)BrPC and (11,12)BrPC for PW_1, PW_5, PW_9, PW_{16} bound to DOPC vesicles in 1 mM Tris, pH 7.1 at 30°C, probe (mol mol^{-1}) percentage: 30%

Peptides	Quenching efficiencies F_0/F		
	(6,7)BrPC	(9,10)BrPC	(11,12)BrPC
PW1	2.0	2.6	1.7
PW5	2.5	2.6	2.0
PW9	2.3	2.3	1.8
PW16	1.9	2.7	1.8

F and F_0 are the peptide fluorescence in the presence and in the absence of brominated probes, respectively.

In this way, for a given probe, whatever the Trp residue considered, the ratio $\sigma = \delta/\ell$ remains constant. In this expression, δ denotes the distance between a phosphorus atom and a bromine one, ℓ is the distance between the ith Trp and $i+1$ or $i-1$ lysine residue; the latter can be roughly estimated from $\ell = 2\pi r\theta/360 = 10.5$ Å with $r = 6$ Å radius of the right-handed α helix and $\theta = 100°$ the angle measured on the Edmondson wheel between the ith Trp and $i+1$ or $i-1$ lysine residue (Fig. 10). When $\sigma = 1$ the quenching is maximum.

Thus, for each Trp residue substituted for a leucine in positions $i = 1$, $i = 5$, $i = 9$, $i = 16$, one can always associate a brominated lipid molecule anchored to a lysine residue in positions $i = 2$, $i = 6$, $i = 10$, $i = 17$. Consequently for any of these Trp residues the quenching by a given probe will be identical. The distance δ estimated for the three probes from X-ray data [41,42] are 8.7, 11.2 and 13.2 Å, respectively. This means (Fig. 10) that whatever its position in the

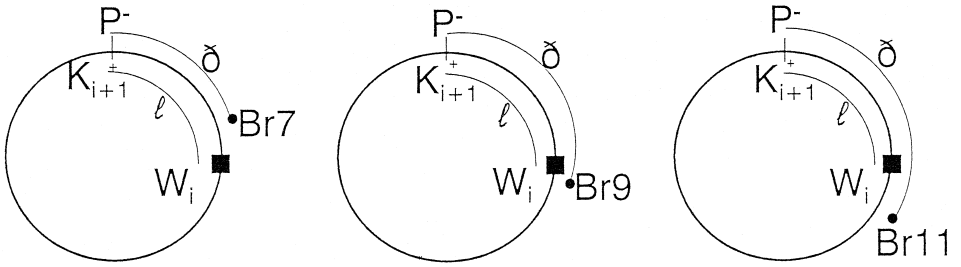

Fig. 10. Sketch representing the quenching of tryptophan by: (a) (6,7)BrPC, ð = 8.71, 10.5 Å; (b) (9,10)BrPC, ð = 11.2 Å; (c) (9,10)BrPC, ð = 13.2 Å.

α helix a Trp residue is always flanked by the (6,7)BrPC or (9,10)BrPC probes, thus the quenching efficiency of each of them should be similar.

The parallax method [43], which allows one to determine the distance of a fluorophore from the center of the bilayer using quenching groups covalently bound at defined positions on lipid acyl chains, requires knowing the distance of these groups from the bilayer center. Due to electrostatic interactions between phosphate groups and lysine residues, such a distance cannot be determined thus precluding the use of the parallax method.

On the other hand, when considering a static quenching, the number n of lipids close enough to the fluorophore can be determined [8] using the relationship:

$$\log(F/F_0) = n \log(1 - x) \quad (2)$$

where x denotes the molar fraction of lipid quencher. We have established the static nature of the Trp quenching by brominated lipid probes, i.e., no temperature dependence of the fluorescence yield and no variation in the three Trp decay times with the quencher concentration. An example of the experimental determination of n is given in Fig. 11. In the case of peptides PW_1, PW_5, PW_9 and PW_{16}, the best fit of Eq. (2) results in a value of n comprised between 2 and 2.5. This corresponds to a ring of lipid molecules surrounding the α helix of about 20–25, i.e., 2–2.5 lipid molecules per lysine residue, such a number being in agreement with the one proposed previously [3].

3.10. Modeling

Since the penetration depth of peptides could not be determined by the parallax method, we attempted to estimate this parameter by molecular modeling simulations.

In Fig. 12, the total energy of the peptide/lipid system together with the shift in peptide location (difference between the final d_f and the initial d_i distances) is plotted vs. d_f (final distance between the

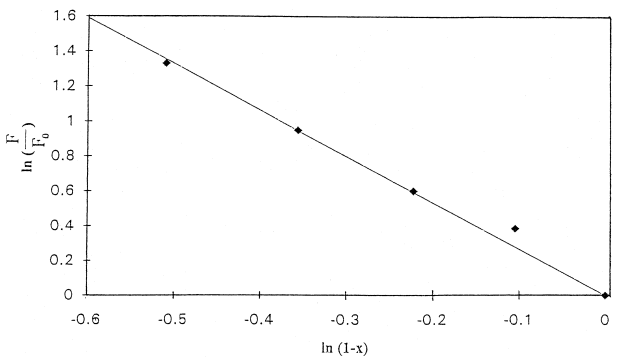

Fig. 11. Determination of the phospholipid molecule mean number associated with PW_5 in a DOPC SUV suspension. $\log(F/F_0)$ vs. $\log(1 - x)$; F_0, flourescence in the absence of quencher; F, fluorescence in the presence of (9,10)BrPC quencher; x, quencher percentage.

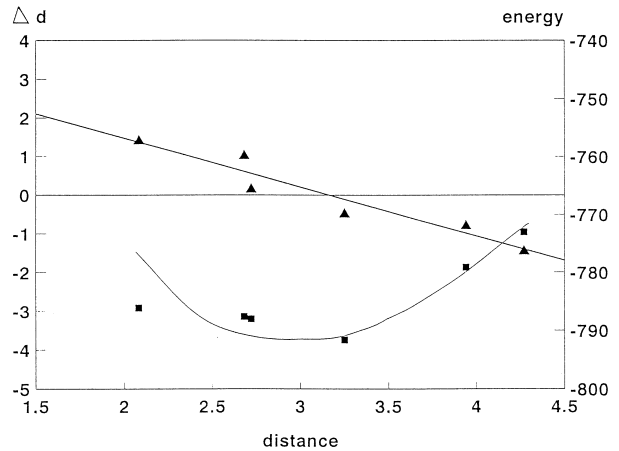

Fig. 12. Energy (▲) of a 24 lipid/peptide assembly and $\Delta d = d_f - d_i$, (■) plot vs. final penetration depth d_f.

peptide centroid and the reference plane). The energy curve exhibits a minimum for a distance $d_f = 3.2$ Å, and there is no shift in peptide location for an initial distance d_i equal to this value. Fig. 13 is a snapshot of the molecular arrangement in the final structure corresponding to the optimum peptide driving in, whereas the corresponding sketch is drawn in the insert.

One of the typical features exhibited by this molecular model is the following: the leucine residues are embedded in the hydrophobic region of the monolayer. The peptide penetration depth into the outer layer, relative to the reference plane defined from the coordinates of the phosphorus atoms belonging to the unperturbed lipid area, reaches an optimum value of 3.2 Å.

The other typical feature of the model concerns the lipid choline groups. In an unperturbed monolayer the P–N segment of the polar head lies nearly parallel to the membrane: from neutron scattering experiments [44,45], the distance measured along the monolayer normal between the C_α and the C_γ carbon atoms of the choline is less than 1 Å in the gel phase as well as in the liquid crystalline one. Therefore, the total thickness of the head area above the reference plane of the P atoms could be estimated to be in the range 3–5 Å [46]. As we can see in Fig. 13, when the peptide is embedded in the outer lipid leaflet, the

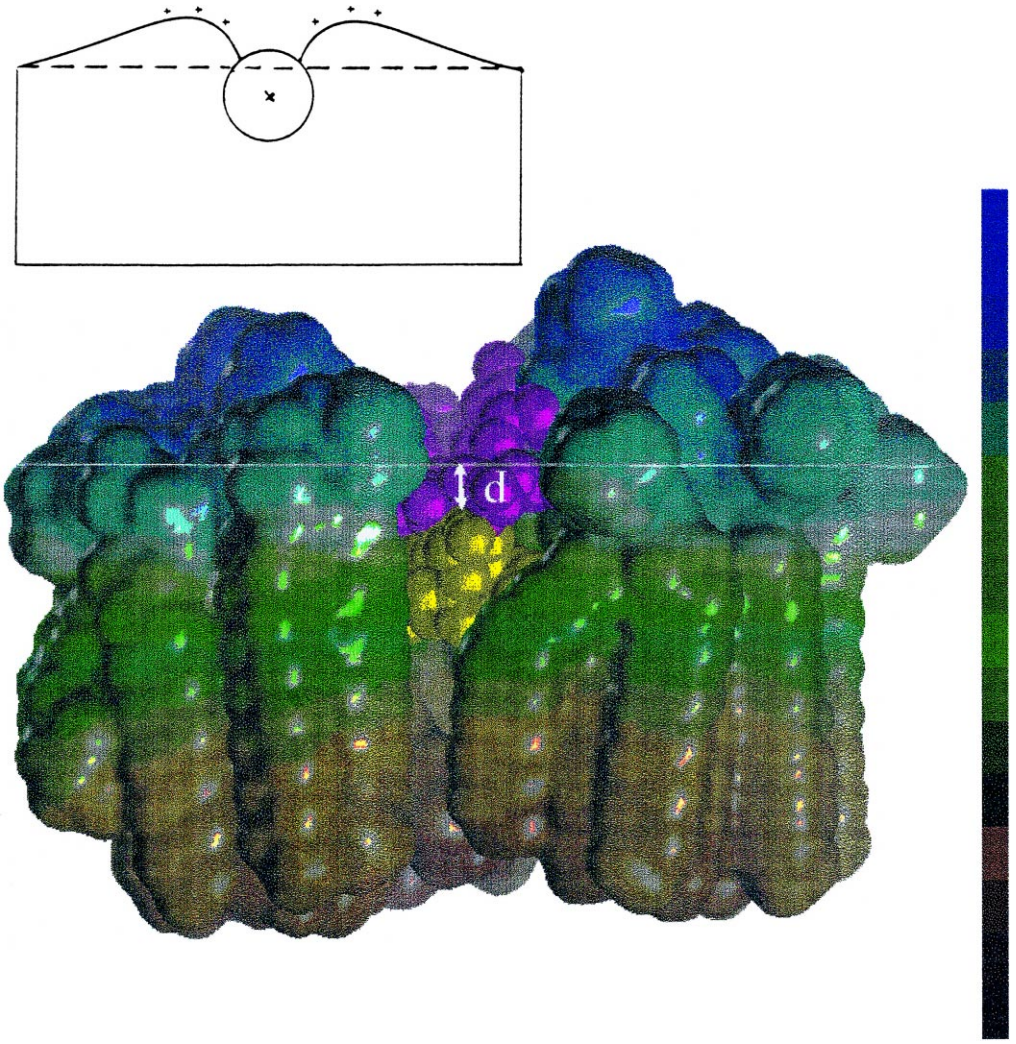

Fig. 13. Peptide/lipids assembly. The lipids are presented as MOLCAD electron density surfaces colored by lipophilicity according to the scale on the left; the helical peptide with normal axis is represented by spacefill atoms colored by residue type (leucine in yellow, lysine in magenta). Insert: sketch illustrating the penetration of the peptide into the lipid layer.

choline methyls in the vicinity of the peptide protrude from the bilayer towards the solvent because of the preferred electrostatic interactions between the lipid phosphate and the protonated amino groups of the peptide lysine residues. This observation is to be related to previous NMR results on acetyl-$(LKKL)_4$-amide bound to DMPC vesicles [2] which showed precisely that the choline methyl groups were not involved in the interaction between peptide and lipid bilayer. The model sketched in Fig. 13 emphasizes the presence of positively charged free choline methyls protruding from the peptide perturbed areas of the membrane towards the solvent. One can surmise that such a situation can favor membrane aggregation, a prerequisite step in the membrane fusion process [47]. Such aggregation and fusion processes were brought out in the case of amphiphilic cationic peptides interacting with DMPC SUVs [2].

3.11. Influence of the transmembrane potential

As indicated in Section 2, egg yolk PC LUVs with bound peptides exhibiting a K^+/Na^+ gradient experienced an inside-negative transmembrane potential $\Delta\psi$. This potential induced by the addition of a minute amount of valinomycin (1 μg PC μmol^{-1}) was estimated at -127 mV from Nernst equation. During the processing of the experiments it was necessary to operate with large ratios of [lipid]/[peptide] ($R_i > 1500$) so that all peptides should be totally membrane bound and vesicle aggregation–fusion phenomena could be neglected. This requirement was a prerequisite to limit light scattering drawbacks and to maintain a steady state transmembrane potential for a while permitting the fluorescence experiments to be carried out. As a matter of fact, probably due to the membrane permeability enhancement to sodium ions involved by the peptide binding, the transmembrane potential tended to decrease and vanish after a few minutes.

Fig. 14 shows the K^+ diffusion potential influence on fluorescence properties of the four Trp-containing peptides. Despite an appreciable margin of error in the determination of both maximum emission wavelength (± 3 nm) and fluorescence intensity, the transmembrane potential resulted in increased emission intensity which was accompanied by a blue shift of the maximum emission wavelength comprised between 4 and 7 nm depending on the peptide. These results indicate that the tryptophan entered a different, more hydrophobic environment. Such behavior is hardly compatible with a flip of the peptide molecules which would lead to a perpendicular reorientation of the helix axis in relation to the membrane surface. In fact, if it was so, either there would have been no variation of the fluorescence parameters since the α helix should maintain its own lipid environment, or possibly, in the case where the α helix spanned the bilayer, the PW_1 Trp residue would pass from a hydrophobic environment to a less hydrophobic one. And this is not what is experimentally observed since each of the fluorescence parameters, yield and emission maximum wavelength, evolved in the same way.

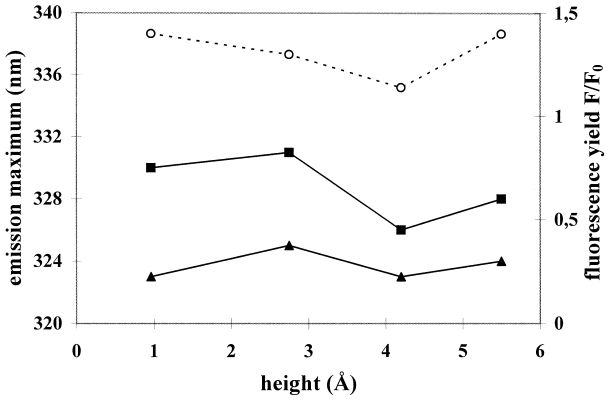

Fig. 14. Influence of the K^+ diffusion potential on fluorescence parameters (emission maximum wavelength, fluorescence yield) of peptides PW_1, PW_5, PW_9 and PW_{16} bound to egg yolk PC LUVs, [lipid]/[peptide] = 1700; the peptides are referred to by their height (see Fig. 6B). ■: emission maximum wavelength in the absence of potential, ▲: emission maximum wavelength in the presence of a diffusion potential $\Delta\psi$ estimated at ~ -127 mV, ○: fluorescence yield F/F_0 with F, fluorescence intensity in the presence of a diffusion potential and F_0 fluorescence intensity in the absence of potential.

In the experiments described herein, everything happens as if peptides suffered an inwards translation movement, the α helix axis remaining parallel to the membrane surface. Clearly this movement was rapidly counterbalanced by hydrophobic forces which prevented the positive charges on lysine residues from penetrating into the hydrophobic region and by electrostatic interactions with phosphate groups which tended to maintain the lysine residues in the hydrophilic region.

4. Discussion

Amphiphilic cationic peptides are known as efficient agents having an antibacterial activity. Accumulating data suggest that peptide–lipid interactions appear to be an essential step in the membrane permeation; however, the precise mechanism of this activity is not yet well known. Here, we have synthesized a cationic amphiphilic peptide containing 10 lysine and 10 leucine residues, and four fluorescent derivatives where leucines were substituted by Trp at different locations on the primary sequence.

This study was undertaken with the aim of eliciting information concerning the conformation, the orientation, the depth of penetration, the sensitivity to electrical potential and the lipid packing disturbing effect of cationic amphiphilic α helical peptides embedded in model phospholipid membranes.

The experimental data presented here show that all the five peptides examined interact with neutral and anionic lipid vesicles made up of DMPC, DMPG, DOPC or egg yolk PC. The binding takes place whatever the peptide conformation in solution(random-coil or α helix aggregates). In the case of DMPC bilayers the binding energy ΔG was estimated at -8 kcal mol^{-1} and the number of phospholipids involved in the interaction close to 20–25 per peptide molecule. Peptides are bound as single stranded α helices which are oriented parallel to the bilayer surface and the electrostatic interactions between lysine and phosphate groups [2] play a key role since when they do not occur as is the case in DMTAP bilayers, peptide binding is not possible. This suggests a two-step insertion mechanism involving prerequisite electrostatic interactions and then clustering of the leucine residues driven by hydrophobic forces into the membrane interior.

The data concerning the static quenching by brominated lipid probes of the four fluorescent peptide derivatives evidenced that, for a given probe, the quenching efficiency remained constant whatever the peptide investigated. We have shown that this can be accounted for by a particular anchoring of the phospholipid head groups in relation to the peptides: these lipid molecules are not smeared out in a plane parallel to the membrane surface but they become organized around the hydrophilic face of the α helices like ‘wheat grains around an ear’, leading to marked mobility reduction of leucine residues by steric hindrance. This conclusion is supported by the NMR spectra of Trp containing peptides bound to SUVs, where the Trp resonance signals practically vanish (results not shown). Consequently, as explained above, the parallax method using brominated lipid probes failed to determine the penetration depth of the fluorescent peptides in lipid bilayers. This type of lipid organization around the peptide helices, comparable to a solvation phenomenon, results in a strong perturbation of the outer leaflet by disrupting the lipid layer and this, in turn, generates numerous transient structural defects. A similar phenomenon concerning the interactions of Cecropin P, a positively charged antibacterial peptide, with phospholipid vesicles has been described [48] and the concept of structural defects in lipid bilayers has already been proposed by several authors [38,39] to explain the membrane permeability induced either by osmotic shock or electrical potentials. It can be thought that peptide-induced structural defects such as these are responsible for the membrane permeability enhancement and can enable the passage of ions or low molecular weight molecules.

Our proposal is also supported by the conclusions which can be inferred from the potential influence on the peptide orientation inside the bilayer. Thus, with applied potential, the data strongly suggest that the axis of the peptide helix remains parallel to the membrane surface and does not reorient to give rise to a bundle of helix monomers that form transmembrane channels via a barrel stave mechanism. We think that such an interpretation could also be applied to several cationic amphipathic peptides which possess lytic and/or antimicrobial activity [4–7].

Using the combination of minimization and simulated annealing techniques of molecular modeling, we presented a picture of a peptide embedded in a lipid layer and we estimated the penetration depth of the peptide. In Fig. 13, we can observe that the amphipathic peptide binding makes the outer lipid layer thickness decrease locally and the choline moieties point towards the solvent. This effect can be related to the mattress effect [49] described for peptides spanning the bilayer.

The penetration depth results can be compared with more elaborate molecular dynamics simulations on the interaction between a DOPC bilayer and an

amphiphilic peptide part of the Corticotropin Releasing Factor [50]. This peptide oriented parallel to the bilayer surface is located on the top of the head groups after a 510-ps simulation. However, in this case the lower penetration depth could be explained by the lower number of positively charged residues and the presence of negatively charged Glu residues which could interact with the outer choline moieties.

In summary, the modeling study gives equilibrium mean values which are consistent with the global information extracted from other experiments and with what we know about the partitioning of peptide in lipid bilayers [51].

References

[1] I. Cornut, E. Thiaudiere, J. Dufourcq, in: R.M. Epand, (Ed.), The Amphipathic Helix, CRC Press, USA, 1993, pp. 173–217.
[2] J.A. Reynaud, J.P. Grivet, D. Sy, Y. Trudelle, Biochemistry 32 (1993) 4997–5008.
[3] J.A. Reynaud, D. Sy, Bioelectrochem. Bioenerg. 34 (1994) 1–4.
[4] S.E. Blondelle, R.A. Houghten, Biochemistry 31 (1992) 12688–12694.
[5] I. Cornut, K. Büttner, J.L. Dasseux, J. Dufourcq, FEBS Lett. 349 (1994) 29–33.
[6] M. Dathe, M. Schumann, T. Wieprecht, A. Winkler, M. Beyermann, E. Krause, K. Matsuzaki, O. Murase, M. Bienert, Biochemistry 35 (1996) 12612–12622.
[7] T. Kiyota, S. Lee, G. Sugihara, Biochemistry 35 (1996) 13196–13204.
[8] E. London, G.W. Feigenson, Biochemistry 20 (1981) 1932–1938.
[9] C. Huang, J.T. Mason, Proc. Natl. Acad. Sci. U.S.A. 75 (1978) 308–310.
[10] M.J. Hope, M.B. Bally, G. Webb, P.R. Cullis, Biochim. Biophys. Acta 812 (1985) 55–65.
[11] R. Maget-Dana, M. Ptak, Biophys. J. 68 (1995) 1937–1943.
[12] A.S. Waggoner, Annu. Rev. Biophys. Bioenerg. 8 (1979) 47–68.
[13] Y.H. Chen, J.T. Yang, K.H. Chau, Biochemistry 13 (1974) 3350–3359.
[14] Ph. Wahl, in: M. Pain, B. Smith (Eds.), New Techniques in Biophysics and Cell Biology, Vol. 2, Wiley, London, 1975, p. 233.
[15] D.V. O'Connor, D. Philips, Time-Correlated Single Photon Counting, Academic Press, London, 1984.
[16] J.C. Brochon, P. Tauc, F. Merola, B.M. Schoot, Anal. Chem. 65 (1993) 1028–1034.
[17] A.K. Livesey, J.C. Brochon, Biophys. J. 52 (1987) 693–706.
[18] J.C. Brochon, Methods in Enzymology, Chap. 13, Vol. 240, Part B, (1994), pp. 262–311.
[19] C.A. Laughton, Prot. Eng. 7 (1994) 235–241.
[20] Mangavel et al., to be published.
[21] S.Y.M. Lau, A.K. Taneja, R.S. Hodges, J. Biol. Chem. 259 (1984) 13253–13261.
[22] L.G. Melton, F.C. Church, B.W. Erickson, Int. J. Peptide Protein Res. 45 (1995) 44–52.
[23] S. McLaughlin, H. Harrary, Biochemistry 15 (1976) 1941–1948.
[24] G. Beschiasvili, J. Seelig, Biochemistry 21 (1990) 52–58.
[25] S. Stankowski, Biochim. Biophys. Acta 735 (1983) 341–351.
[26] M. Vankann, M. Federwisch, J. Mölerfeld, H. Höcker, J. Colloid Interface Sci. 173 (1995) 460–470.
[27] J.R. Lakowicz (Ed.), Principles of Fluorescence Spectroscopy, Plenum, New York, 1983.
[28] N.J. Turro, M. Aiqawa, A. Yekta, Chem. Phys. Lett. 64 (1979) 473–475.
[29] D.P. Millar, Curr. Opin. Struct. Biol. 6 (1996) 637–642.
[30] R.F. Chen, J.R. Knutson, H. Ziffer, D. Porter, Biochemistry 30 (1991) 5184–5195.
[31] E.S.T. Dahms, K.J. Willis, A.G. Szabo, J. Am. Chem. Soc. 117 (1995) 2321–2326.
[32] J.B.A. Ross, H.R. Wyssbrod, R.A. Porter, G.P. Schwartz, C.A. Michaels, W.R. Laws, Biochemistry 31 (1992) 1585–1594.
[33] K.J. Willis, A.G. Szabo, Biochemistry 31 (1992) 8924–8931.
[34] Y. Chen, B. Liu, H.T. Yu, M. Barkley, J. Am. Chem. Soc. 118 (1996) 9271–9278.
[35] R.W. Cowgill, Biochim. Biophys. Acta 133 (1967) 6–18.
[36] A. Chattopadhyay, S. Mukherjee, Biochemistry 32 (1993) 3804–3811.
[37] A.P. Demchenko, Ladokhin, Eur. Biophys. J. 15 (1988) 369–379.
[38] I.G. Abidor, V.B. Arakelyan, L.V. Chernomordik, Y.A. Chizmadzhev, V.F. Pastushenko, M.R. Tarasevich, Bioelectrochem. Bioenerg. 6 (1979) 37–52.
[39] C. Taupin, M. Dvolaitzky, C. Sauterey, Biochemistry 14 (1975) 4771–4775.
[40] J.M. East, A.G. Lee, Biochemistry 21 (1982) 4144–4151.
[41] B.A. Lewis, D.M. Engelman, J. Mol. Biol. 166 (1983) 211–217.
[42] T.J. McIntosh, P.W. Holloway, Biochemistry 26 (1987) 1783–1788.
[43] A. Chattopadyay, E. London, Biochemistry 26 (1987) 39–45.
[44] G. Büldt, H.U. Gally, J. Seelig, G. Zaccai, J. Mol. Biol. 134 (1979) 217–673.
[45] G. Büldt, J. Seelig, Biochemistry 19 (1980) 6170–6175.
[46] J.N. Israelachvili, S. Marcelja, R.G. Horn, Q. Rev. Biophys. 13 (1980) 121–200.
[47] J.H. Prestegard, M.P. O'Brien, Annu. Rev. Phys. Chem. 38 (1987) 383–411.
[48] E. Gazit, A. Boman, H.G. Boman, Y. Shaï, Biochemistry 34 (1995) 11479–11488.
[49] O.G. Mouritsen, M. Bloom, Biophys. J. 46 (1984) 141–153.
[50] G.P. Huang, G.H. Loew, J. Biomol. Struct. Dyn. 12 (1995) 937–956.
[51] S.H. White, W.C. Wimley, Curr. Opin. Struct. Biol. 4 (1994) 79–86.